Multi-scale identification of the elastic properties variability for composite materials through a hybrid optimisation strategy

Lorenzo Cappelli, Georgios Balokas, Marco Montemurro, Frédéric Dau, Laurent Guillaumat

Version of Record: https://www.sciencedirect.com/science/article/pii/S1359836819321766
Manuscript_1a7e0a987ed03a064e38b46bfb230b2c

Multi-scale identification of the elastic properties variability for composite materials through a hybrid optimisation strategy

Lorenzo Cappelli[a], Georgios Balokas[b], Marco Montemurro[a,*], Frédéric Dau[a], Laurent Guillaumat[c]

[a] *Arts et Métiers ParisTech, Institut de Mécanique et d'Ingénierie (I2M) de Bordeaux CNRS UMR 5295, F-33400 Talence, France*
[b] *Structural Optimization for Lightweight Design, Hamburg University of Technology, Hamburg, Germany*
[c] *Arts et Métiers ParisTech, Laboratoire Angevin de Mécanique, Procédés et innovAtion (LAMPA), F-49100 Angers, France*

Abstract

The problem of the identification of the variability characterising the elastic properties of the constitutive phases of a composite (at the microscopic scale) is addressed in this work. To this purpose, the information contained into the probability distribution of the first buckling load of a macroscopic composite specimen is considered, in order to develop a multi-scale identification strategy (MSIS).

The goal of the proposed MSIS is achieved by solving an inverse problem: the minimisation of the distance between the numerical and the reference buckling response of the plate, at the macroscopic scale, in terms of statistical moments. Furthermore, thermodynamic constraints are considered to ensure the positive definiteness of the stiffness tensor of each constituent of the composite.

The proposed strategy relies on: (a) a semi-analytical homogenisation method, to perform the microscopic / mesoscopic scale transition; (b) the Monte-Carlo technique and an Artificial Neural Network to determine the material properties variability; (c) a general hybrid optimisation algorithm able to deal with optimisation problems defined over a domain of variable dimension to perform the solution search. The effectiveness of the MSIS is proven through two meaningful benchmarks.

Keywords: Composite materials, Homogenisation, Buckling, Uncertainty quantification, Surrogate model, Inverse problems, Optimisation

1. Introduction

Composite materials are nowadays widely used into mechanical components or engineering systems and structures belonging to different fields: from automotive to aerospace, from naval to biomedical. They are mainly employed due to their outstanding strength-to-weight and stiffness-to-weight ratios: these features are of paramount importance for lightweight applications, such as aircraft and space vehicles architectures [1]. Composites can be used to build integrated structures because both stiffness and strength can be tailored point-wise according to the requirements of the problem at hand. This feature allows

*Corresponding author. Tel.: +33 55 68 45 422, Fax.: +33 54 00 06 964.
Email address: marco.montemurro@ensam.eu, marco.montemurro@u-bordeaux.fr (Marco Montemurro)

for preserving structural continuity without introducing complex structural elements (and the related manufacturing aspects) by opportunely meeting geometrical and mechanical design requirements.

In the literature, research studies exploiting refined numerical and experimental techniques are increasingly used to characterise the mechanical behaviour of composite materials [2–4]. Nevertheless, especially in large-scale production, a large amount of uncertainty arises from unavoidable manufacturing imperfections for both geometrical and material properties. Intralaminar and/or matrix voids, excess of resin between adjacent laminae and incomplete cure of resin are only some examples: environmental factors and uncertain operational aggravate this issue.

As outlined in [5], the uncertainties are classified in three main categories: aleatory (variability of structural parameters), epistemic (lack of adequate information about the system) and prejudicial (absence of stochastic characterisation of the structural system). Composite structures are affected by all three forms of uncertainty and the characterisation of parameters tuning the variability law becomes of prime importance. However, experimental methods commonly used to characterise the material properties require a huge number of standard ASTM tests, if used for uncertainty characterisation, which are destructive and expensive [6]. Moreover, these tests are only suited to evaluate mesoscopic uncertainties, in terms of material and geometrical properties of the lamina without providing any information about the variability characterising the properties of the constitutive phases at the microscopic scale.

Standard tests that can be carried out at the mesoscopic scale include the tension test for flat specimens (ASTM D3039 [7]), the three/four points bending test (ASTM D790 [8]), the compression tests (shear loading methods ASTM D3410 [9]) and the shear tests (in-plane shear tests ASTM D5379 [10]-D7078 [11]-D3518 [12], out-of-plane - interlaminar shear tests ASTM D2344 [13]-D5379). As far as the microscopic scale is concerned, only few standard experimental tests can be found in the literature: single fibre tensile test (ASTM D3379 [14]) and matrix tensile test (ASTM D638 [15]) to characterise the Young's elastic modulus of the fibre in the longitudinal direction and that of the matrix, respectively. In order to characterise the rest of the constitutive phases elastic properties only non-standard tests are available in the literature: pull-out [16], micro-indentation [17], fragmentation tests [18], etc. These tests are not able to evaluate the full 3D set of the material properties of the constituents and they are very difficult to be carried out, due to the fibres diameter size.

In order to get statistically representative results, the aforementioned tests must be performed a huge number of times. Of course, this implies significant costs (and time) and the variability results (e.g. mean and standard deviation of material properties) are strongly affected by the errors introduced to carry out the experimental campaign, especially for those tests conducted at the microscopic scale. To this purpose, Sepahvand *et al.* developed the inverse stochastic method based on the general polynomial chaos (gPC) [19–25] to identify uncertain lamina elastic parameters from experimental modal data. Further examples of probabilistic methods are the parametric probabilistic approach [26] and the Bayesian inference techniques wherein all information are included into a prior distribution model [27–30]. However, in the case of composite structures, the uncertainty affecting the ply elastic behaviour is strictly related to the variability of the elastic properties of the constitutive phases. To the best of the authors' knowledge, only few works on the identification of the variability parameters characterising the material properties of the microscopic constituents of the composite are available in the literature [31]. The majority of researches in this field are devoted to the characterisation of the material properties

uncertainty parameters at the ply-level [32–35].

The research activity here presented focuses on the development of a multi-scale identification strategy (MSIS) which smartly exploits the data resulting from macroscopic buckling tests to characterise the uncertainty of the constitutive phases elastic properties at the microscopic scale. The proposed MSIS has been initially proposed in [36] to identify the elastic properties of the composite (at each relevant scale), starting from the harmonic response of the multilayer composite plate at the macroscopic scale. Here, the MSIS is extended to the multi-scale characterisation of the variability related to the elastic properties at the microscopic scale of the composite.

The MSIS is characterised by some original features. Firstly, it relies on a particular hybrid optimisation tool used to perform the solution search, which is an in-house code made by the union of a special genetic algorithm (GA), i.e. ERASMUS (EvolutionaRy Algorithm for optimiSation of ModU- lar Systems) developed by Montemurro [37] (which is able to deal with problems characterised by a number of design variables that can change during the optimisation process [38]) and of a gradient-based one, belonging to the MATLAB®*fmincon* family [39]. Secondly, the MSIS makes use of the Chamis's micro-mechanical model [40, 41] to perform the microscopic / mesoscopic scale transition. Finally, the MSIS makes use of the Monte Carlo framework that allows describing the statistical nature of the elastic response. To improve the efficiency of the Monte Carlo technique (i.e. to minimise the computational effort related to such a method), an Artificial Neural Network (ANN) [41] is developed as a surrogate model: the probability distribution of the first buckling load is predicted starting from the probability density functions of the elastic properties of the constituent phases. The effectiveness of the MSIS is proven by means of two meaningful benchmarks.

Concerning the state-of-the-art of the approaches combining optimisation and uncertainty, three specific research areas can be identified in the literature, as outlined in [42]: reliability-based optimisation (RBO), robust design optimisation (RDO) and model updating. The RBO technique concerns the solution of an optimisation problem in which the main goal is to design for safety by considering extreme events: common objective functions are defined by the structural weight and the constraints are both deterministic and probabilistic (e.g. probability of failure of the structure) [43–46]. The RDO method is usually implemented in order to minimize the influence of stochastic variations on the mean design [47]. Finally, the typical goal of the model updating technique is to reduce the differences between model prediction and data from tests [48, 49]. In this context, the MSIS can be considered as a model updating technique that allows identifying the elastic properties of the composite (and the related uncertainty) at each scale. This information can be later used in the framework of both RBO and RDO approaches.

The paper is organised as follows. The problem description and the MSIS are presented in Section 2. The analytical and the finite element (FE) models developed at each pertinent scale are shown in Section 3. The uncertainty microscopic quantification with the Monte-Carlo technique and the implemented ANN are described in Section 4. The sensitivity analyses concerning the meta-model of the considered benchmarks are presented in Section 5, while the mathematical formulation of the inverse problem is discussed in Section 6. The numerical results provided by the MSIS are given in Section 7. Finally, Section 8 ends the paper with conclusions and perspectives.

2. Multi-scale identification of the variability of composite elastic properties

2.1. The multi-scale identification strategy

The goal of the MSIS is the characterisation of the variability related to the elastic properties of the microscopic constituents of the composite, by using only the information contained into the statistical sample of the first buckling load of the multilayer plate at the macroscopic scale. In this way, only cheap, standard tests have to be realised at the macroscopic scale, with the main advantage of reducing the characterisation time, the associated costs and the necessity of specialised skills.

The *reference* macroscopic response can be evaluated either by means of an extensive experimental campaign of buckling tests or through a wide numerical campaign of tests on a reference configuration of the multilayer plate. To prove the effectiveness of the MSIS, this latter case has been considered in this work.

To this purpose, the problem of characterising the variability related to the elastic properties of the fibre and the matrix is stated as a multi-scale constrained inverse problem. Of course, the numerical models involved in the MSIS are characterised by some fundamental hypotheses. As far as the microscopic scale is concerned, the main hypotheses are: (a) linear elastic isotropic behaviour for the matrix; (b) linear elastic transversely isotropic behaviour for the fibre; (c) the matrix / fibre interface is perfect; (d) the damping capability of both phases is neglected; (e) the uncertainty of the elastic properties is described by means of a Gaussian probability distribution.

At the laminate macroscopic scale the following hypotheses hold: (a) the constitutive lamina has a linear elastic transversely isotropic behaviour; (b) the interface between two adjacent plies is perfect; (c) the damping capability of the lamina is neglected; (d) the kinematics of the laminate is described by the first-order shear deformation theory (FSDT).

The general flow chart of the MSIS is illustrated in Figure 1. The details of the optimisation algorithms employed within the MSIS are given in [36, 37].

2.2. Problem description

The proposed multi-scale inverse approach for uncertainty characterisation is here applied to a reference multilayer composite plate made of unidirectional laminae: the relevant geometrical parameters are shown in Figure 2. Two different benchmarks are investigated to evaluate the identification capability of the proposed MSIS. In particular the geometry of the reference laminate is the same for both cases, the only difference being the considered stacking sequence, i.e.

- benchmark 1 (BK1) $[0°/-45°/45°/90°]_S$;
- benchmark 2 (BK2) $[45]_8$.

For both laminates, the thickness of the elementary lamina is $t_{\text{ply}} = 0.282$ mm. The orientation angle of the generic ply is positive according to counter-clockwise rotation around the z-axis: the x-axis indicates the 0° orientation, as illustrated in Figure 2.

The constitutive ply is made of carbon-epoxy fibre-reinforced Hexcel $T650/F584$ pre-impregnated tapes: its elastic properties are listed in Table 1. The mean values are taken from [50, 51], while the standard deviation and the relative shapes of the probability density functions are not available experimentally for both the microscopic and the mesoscopic material properties. To this purpose, a Gaussian probability density function $\chi_i = \chi_i(x_i)$

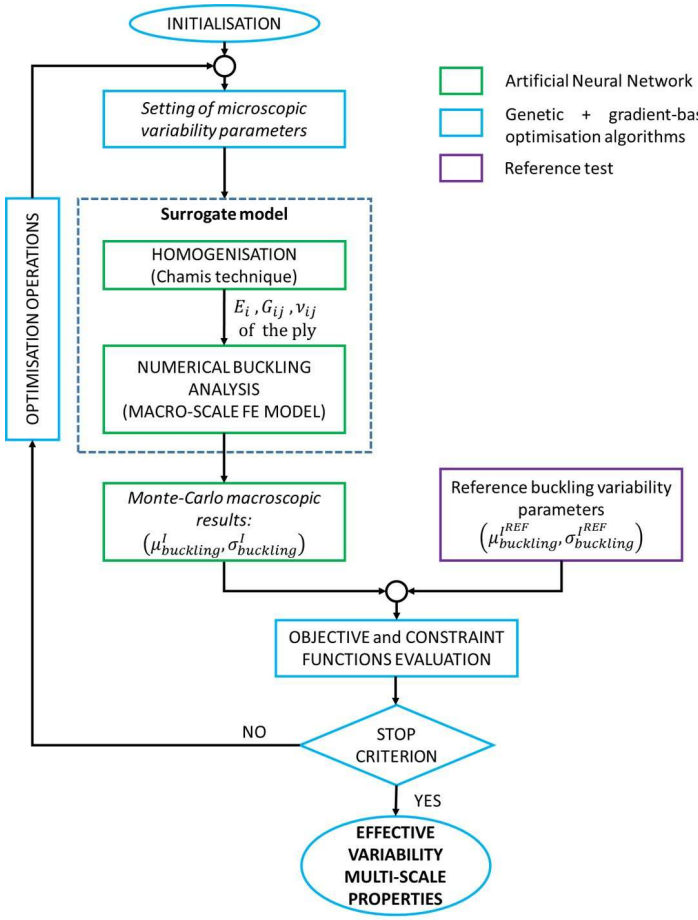

Figure 1: Flow chart of the MSIS.

is selected as a reference distribution for describing the uncertainty of the generic property x_i at the scale of the constituent phases. The analytical formula of such a distribution is

$$\chi_i(x_i) = \frac{1}{\sigma(x_i)\sqrt{2\pi}} e^{\frac{(x_i - \mu(x_i))^2}{2\sigma^2(x_i)}}, \quad \text{with} \quad x_i \in \Re. \tag{1}$$

In particular, the Gaussian distribution involves two parameters, i.e. the mean value $\mu(x_i)$ and the variance $\sigma^2(x_i)$ of the *i-th* material property x_i. If x_{i_j} is the *j-th* value of x_i occurring with a probability p_{i_j}, the relative mean value and the variance can be expressed as:

$$\begin{aligned} \mu(x_i) &= \sum_{j=1}^{N_i} x_{i_j} p_{i_j}, \\ \sigma^2(x_i) &= \mu(\beta_i(x_i)), \\ \beta_i(x_i) &= (x_i - \mu(x_i))^2. \end{aligned} \tag{2}$$

Usually, the coefficient of variation $\mathrm{COV}(x_i)$ is introduced as a standard measure of

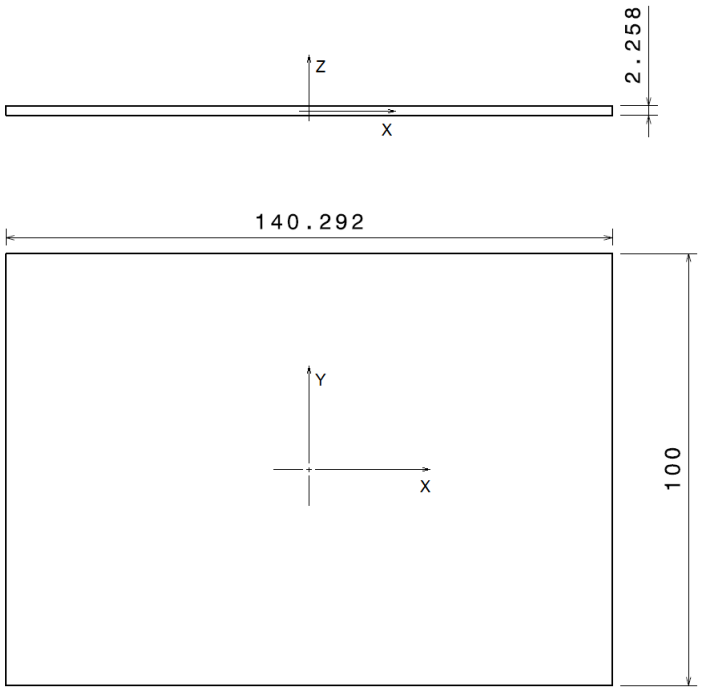

Figure 2: Geometrical parameters of the reference multilayer composite plate (dimensions are in $[mm]$).

the dispersion of the probability distribution function:

$$\mathrm{COV}\left(x_i\right) = \frac{\sigma\left(x_i\right)}{\mu\left(x_i\right)}. \tag{3}$$

	Fibre				Matrix			
	E_1^f [GPa]	E_2^f [GPa]	ν_{12}^f	ν_{23}^f	G_{12}^f [GPa]	E^m [GPa]	ν^m	V_F
$\mu\left(x_i\right)$	276	17.3	0.25	0.428	11.24	4.14	0.35	0.555
$\sigma\left(x_i\right)$	27.6	1.73	0.025	0.0428	1.124	0.414	0.035	0.0555

Table 1: Mean value and standard deviation of the elastic properties for the fibre $T650/35-3K$ and the matrix $F584$ (the mean values are taken from [50, 51]).

In this work, the *reference* distribution of the first buckling load of the structure is determined by means of a multi-scale numerical analysis on the *reference* configuration of the plate for both benchmarks. In particular, the *reference* material properties of the constitutive phases, listed in Table 1, are implemented, firstly, to compute the *reference* distribution of the ply elastic properties. Secondly, the resulting distribution of the lamina elastic properties is used to compute the *reference* distribution of the first buckling load of the composite plate, for each considered benchmark (as described in Section 7.1).

3. Analytical and numerical models at different scales

3.1. Microscopic / mesoscopic scale transition: the Chamis' model

Multi-scale modelling strategies are widely used to assess the behaviour of the composite at each relevant scale [52, 53]. The transition from the scale of the constitutive phases

(microscopic scale) to that of the elementary ply (mesoscopic scale) is performed by means of a homogenisation calculation. This phase can be performed either numerically, e.g. by implementing the well-known strain energy homogenisation technique of periodic media (SEHTPM) [54], or analytically by using a suitable homogenisation scheme for composites, as the Chamis' model [40]. As discussed in [36], the SEHTPM has already been integrated into the MSIS to determine the equivalent elastic behaviour of general periodic materials with complex microstructures. Despite its general nature, the SEHTPM can be quite time consuming (depending on the problem at hand) since the equivalent elastic properties at the upper scale are the result of six static FE analyses (i.e. the equivalent stiffness tensor of the homogenised material is evaluated column-wise). When dealing with uncertainty quantification, the SEHTPM requires a strong computational effort to evaluate the propagation of the uncertainty from the microscopic scale to the mesoscopic one. Therefore, to reduce the computational cost an efficient analytical homogenisation scheme has been considered in this work, i.e. the aforementioned Chamis' model. Moreover, this choice allows avoiding the integration of further FE model-related parameters like the mesh size. In particular, according to the Chamis' model, the ply engineering constants can be determined as follows:

$$
\begin{aligned}
E_1 &= V_F E_1^f + (1 - V_F)\, E^m, \\
E_2 = E_3 &= \frac{E^m}{1 - \sqrt{V_F}\left(1 - \dfrac{E^m}{E_2^f}\right)}, \\
G_{12} = G_{13} &= \frac{\dfrac{E^m}{2\,(1+\nu^m)}}{1 - \sqrt{V_F}\left(1 - \dfrac{\dfrac{E^m}{2\,(1+\nu^m)}}{G_{12}^f}\right)}, \\
G_{23} &= \frac{\dfrac{E^m}{2\,(1+\nu^m)}}{1 - \sqrt{V_F}\left(1 - \dfrac{E^m\left(1+\nu_{23}^f\right)}{E_2^f\,(1+\nu^m)}\right)}, \\
\nu_{12} = \nu_{13} &= \nu^m + V_F\left(\nu_{12}^f - \nu^m\right), \\
\nu_{23} &= \frac{E_2}{2G_{23}} - 1.
\end{aligned}
\tag{4}
$$

In Eq. (4), E_1^f, E_2^f, G_{12}^f, ν_{12}^f, ν_{23}^f are the elastic constants of the transversely isotropic fibre, while E^m and ν^m are the Young's modulus and the Poisson's ratio of the isotropic matrix. The volume fraction of the fibre is indicated as V_F. Moreover, the homogenised elastic properties of the ply are denoted as E_1, E_2, E_3, G_{12}, G_{13}, G_{23}, ν_{12}, ν_{13}, ν_{23}.

3.2. Mesoscopic / macroscopic scale transition: the finite element model

The distribution of the first buckling load of the multilayer plate is the result of an eigenvalue buckling analysis which is carried out by considering the distribution of the ply elastic properties evaluated by means of the Chamis' model. The FE model is developed

into the Abaqus® environment [55]: the Abaqus® shell layered element S4R having *four* nodes and six degrees of freedom (DOFs) per node has been used to build the FE model of the multilayer plate. The kinematics of the element is described in the framework of the first-order shear deformation theory (FSDT) [1]. Of course, this type of element is well suited to describe the buckling strength of the laminate when its aspect ratio is in the range $[20, 100]$. For the problem at hand the multilayer plate is characterised by an aspect ratio $AR = 44.29$. Figure 3 illustrates the loads and boundary conditions (BCs) for the proposed benchmarks.

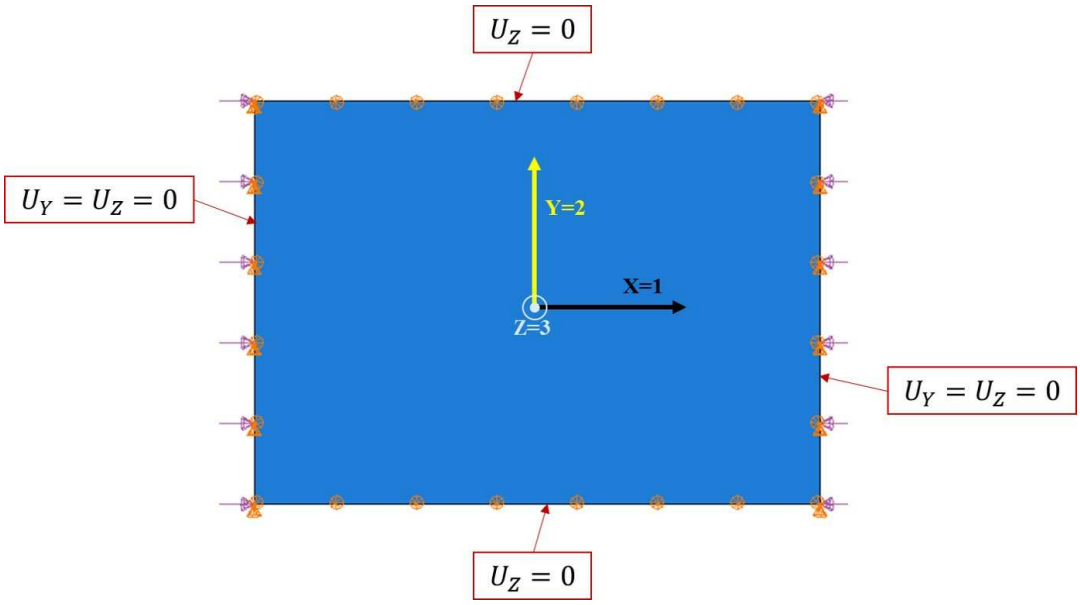

Figure 3: Loads and boundary conditions (BCs) of the macroscopic FE model.

As far as the mesh size is concerned, a sensitivity study of the first buckling load of the laminate to the number of elements (not reported here for the sake of brevity) has been performed: a model with 3654 DOFs is sufficient, to evaluate the first buckling load of the composite plate. The mesh of the FE model is illustrated in Figure 4.

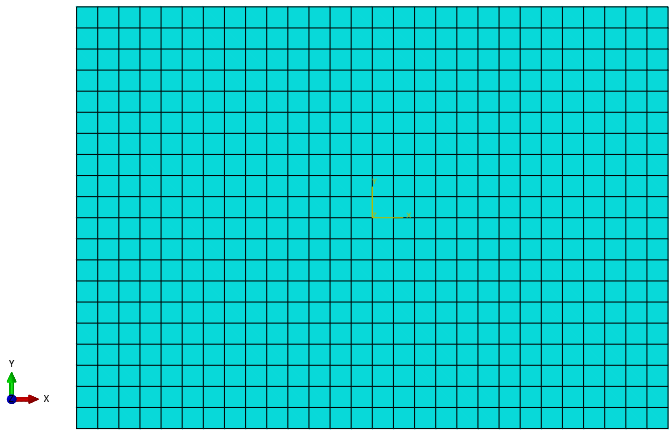

Figure 4: Mesh of the macroscopic FE model.

4. Probabilistic modeling and uncertainty quantification

4.1. Monte Carlo analysis

The Monte Carlo (MC) method [41] is the most straightforward and robust one, among the popular methods used for calculating the response variability in stochastic structural mechanics. Based on the law of large numbers, MC approximates the statistical moments (e.g. mean, variance, etc.) of the quantity of interest (QoI), by performing a sufficient number of model evaluations, while sampling random, independent variables from the input space. The generated finite sample of the QoI is then post-processed, to obtain the unbiased statistics of the response estimates. In mathematical terms, the first and second moment described in Eq. (2) for the discrete case, can be approximated after N realizations as:

$$\begin{aligned} \mu\left(\mathbf{r}\right) &= \frac{1}{N}\sum_{j=1}^{N} r_j, \\ \sigma^2\left(\mathbf{r}\right) &= \frac{1}{N-1}\sum_{j=1}^{N}\left[r_j - \mu(\mathbf{r})\right]^2. \end{aligned} \tag{5}$$

where $\mathbf{r} = \{r_i,\ i = 1, ...N\}$ is the sample of the response QoI (e.g. displacement, force, bucking load etc.). Although MC can practically handle every problem, regardless of the complexity of the response surface topology, the large number of required model evaluations sets the method prohibitive for high-fidelity models (e.g. FE models), especially for applications of reliability or uncertainty quantification.

4.2. Variance-based global sensitivity analysis

In order to understand the cause-and-effect relationship between the input variables and the response, a classification of the random parameters in terms of output variability can be achieved through a global sensitivity analysis (GSA). The total variance of the QoI is decomposed into parts induced from single input parameters, but also potential interactions of the latter. Thus, the uncertain parameters can be qualitatively quantified, and the dominating ones can be later used into the models involved into the optimisation process introduced in Section 6.

Let $f(x_1, x_2, ...\ x_k)$ be a square integrable scalar function over the k-dimensional unit hypercube Ω^{k} model. According to Sobol [56], f can be decomposed into sums of increasing dimensions as follows:

$$f = f_0 + \sum_i f_i + \sum_{j>i} f_{ij} + ... + f_{12...k}, \tag{6}$$

where $f_i = f_i(x_i)$, $f_{ij} = f_{ij}(x_i, x_j)$ etc. After several algrebraic manipulations (the reader is referred to [56] or [41] for details), the final expression for the variance decomposition is reached:

$$\mathrm{Var}(y) = \sum_{i=1}^{k} V_i + \sum_{j>i}^{k} V_{ij} + ... + V_{12...k}, \tag{7}$$

$$\text{where} \quad V_i = \mathrm{Var}_{x_i}(E_{x_{\sim i}}(y|x_i)), \tag{8}$$

$$V_{ij} = \mathrm{Var}_{x_{ij}}(E_{x_{\sim ij}}(y|x_i, x_j)) - V_i - V_j \quad , \text{ etc.} \tag{9}$$

The $x_{\sim i}$ notation indicates the set of all variables except x_i. By dividing the term of interest by the unconditional variance $\mathrm{Var}(y)$, the first-order Sobol index is obtained as a fractional contribution:

$$S_i = \frac{V_i}{\mathrm{Var}(y)}. \tag{10}$$

In the case of non-analytical models, expressions such as Eq. (8) or (9) must be approximated via a sampling (e.g. Monte Carlo) procedure. Firstly, two (N, k) matrices with random samples from the input space are generated, namely A and B, with N being the number of realizations and k the stochastic dimension of the problem. After that, a third matrix A_B^i is formed, identical to A, except its i^{th} column which is replaced by the i^{th} column of B $(i = 1, ..., k)$. Finally, the model is evaluated with respect to the aforementioned input matrices, according to the following estimator for the first-order Sobol index, for every input parameter i:

$$V_i = \mathrm{Var}_{x_i}(E_{x_{\sim i}}(y|x_i)) \approx \frac{1}{N}\sum_{j=1}^{N} f(B)_j(f(A_B^i)_j - f(A)_j). \tag{11}$$

It is noteworthy that there are several other options available, regarding estimators of this sort [56]. A drawback of GSA, is that formulae like Eq. (11) require excessive realizations in order to converge (order of 10^4 or 10^5). In the context of computationally expensive simulations, such as FE analyses, a possible remedy is the emulation of the input-output relationship via a surrogate model, as it is described in the next section.

4.3. Surrogate modelling with Artificial Neural Networks

Surrogate models (or metamodels) are mathematical functions able to mimic the response of a model, when trained with a relatively small training set of model evaluations. Afterwards, the demanding model can be substituted from these inexpensive proxy models, for applications requiring an excessive amount of simulations (e.g. optimization, reliability, GSA etc.) Popular choices, among relevant research studies, are ANNs, Gaussian processes (or Kriging), polynomial chaos expansions (PCE) and support vector machines (SVM), as outlined in [57].

In this work, a surrogate is appropriately trained to emulate the multi-scale modelling strategy described in Section 3. The material properties of the different phases at the micro-scale, listed in Eq. (15), are used as input, while the output response is the plate first buckling load. The aim of the surrogate is twofold. Firstly, it is used for the GSA and the evaluations required by the estimator of Eq. (11). Secondly, as explained in Section 1, it is used into the multi-scale identification strategy to boost the optimisation process. Concerning the surrogate type, ANNs are selected in this study, mostly because, despite their versatility and their good generalization, they only have few parameters to be tuned within their training procedure, which is beneficial for the optimisation algorithm.

In particular, an ANN is a parallel information-processing system, consisting of at least three layers: the input, the output and one (or more) hidden layer. The nodes inside every layer are called *neurons* and they are linked by the so-called *synapses*. When information is circulated only in a single direction, the network is called feed-forward. An illustration of a typical single-layer, feed-forward ANN configuration is shown in Fig. 5. It is noteworthy, that the input neurons (squares) connect the network to the external environment, without further processing information, while the hidden layer neurons (circles) process information from a previous layer and feed it to the next one.

The learning procedure of an ANN is based on a general function optimisation problem, where the weight parameters w_{ij} assigned to every synapse are the design variables, and the objective function is the sum squared error between the predicted output $t(w_{ij})$ and the target output y_0:

$$E(w_{ij}) = \frac{1}{2}\sum[t(w_{ij}) - y_0]^2. \tag{12}$$

During the process, the weights are updated through an iterative procedure, until the desired error level is achieved or the maximum number of cycles is reached:

$$w_{ij}^{(t+1)} = w_{ij}^{(t)} + \Delta w_{ij}, \tag{13}$$

where Δw_{ij} is the correction of the weight at the t^{th} learning step. In order to avoid overfitting, a fraction of the sample data is used as a validation dataset and the error is monitored over the iterations to stop the training early enough. Regarding the internal process in every neuron, each input from the previous neuron is placed into a weighted sum as the following:

$$z_j = \sum_{i=1}^{k} x_i w_{ij} + b, \tag{14}$$

which then goes through an activation function where the nonlinearity of the decision boundary is introduced (usually of sigmoid type). The term b in the previous equation is a bias term allowing the neuron to cover a broader range. For more details on ANNs, the interested reader is addressed to [41].

5. Sensitivity analysis of the meta-model

5.1. Global Sensitivity Analyses for the two benchmarks

The implementation of the Artificial Neural Network, described in Section 4.3, allows to apply the variance-based GSA described in Section 4.2, since the computational effort needed to perform the convergence of the Sobol index is negligible. All the material and

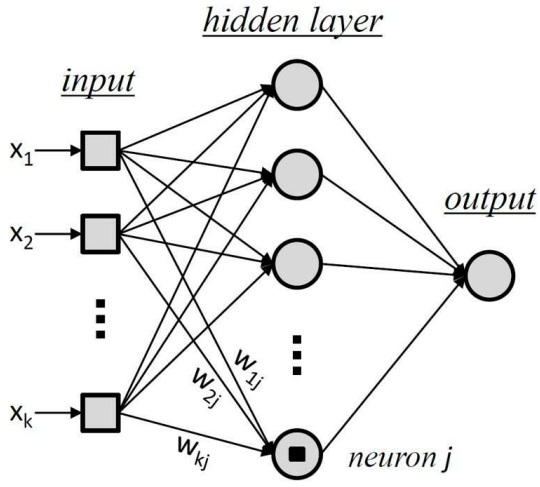

Figure 5: Architecture of a single layer feed-forward neural network.

geometrical variables of the constitutive phases with the related uncertainty are considered here: through the total output variance decomposition, it is possible to identify the dominant microscopic input parameters, from a statistical point of view.

According to the hypotheses given in Section 1, a total of eight variables can be identified for the microscopic constituents of the composite, i.e.

$$\mathbf{x} = \left\{ E_1^f, E_2^f, G_{12}^f, \nu_{12}^f, \nu_{23}^f, E^m, \nu^m, V_F \right\}. \tag{15}$$

The related mean and standard deviation values are summarised in Table 1, in which, a COV equal to 10% is set, for all the parameters concerning the microscopic scale. The causes at the basis of this uncertainty are various and often very difficult to be identified. For example, the uncertainty of the fibre volume fraction is often related to the manufacturing process parameters.

The results of the variance-based GSA for every benchmark are shown in Figures 6a and 7a, in terms of the evolution of the Sobol index, defined in Eq. (11), over the number of simulations. It is possible to observe that the Sobol index converges after around 15000 simulations, for both benchmarks.

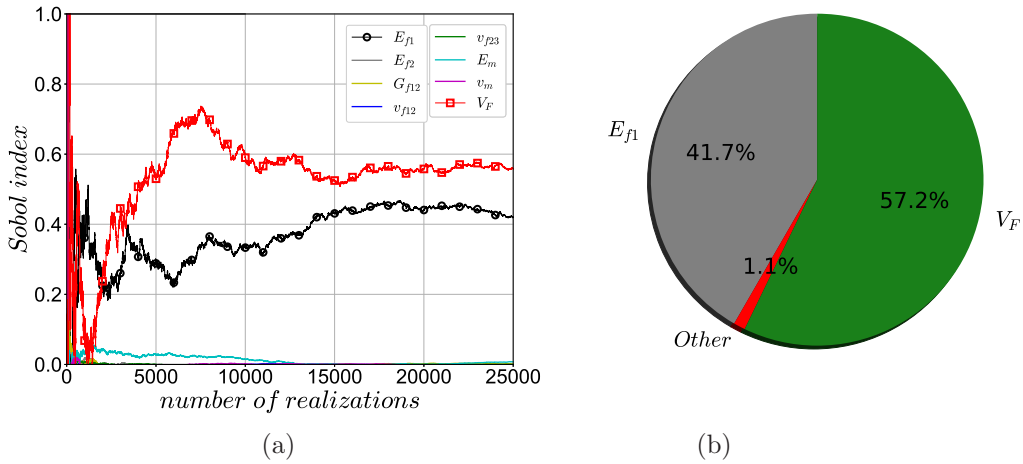

(a) (b)

Figure 6: (a) Convergence of the Sobol index and (b) sensitivity analysis results, for the first benchmark (BK1).

The pie diagrams shown in Figures 6b and 7b highlight a result of paramount importance: the sensitivity of the first buckling load to the material and geometrical properties of the constitutive phases (and the related uncertainty as well) is strongly influenced by the nature of the stacking sequence. In particular, for benchmark BK1, which is characterised by a quasi-isotropic symmetric stack, the sensitivity of the first buckling load to the elastic properties E_2^f, G_{12}^f, ν_{12}^f, ν_{23}^f, E^m, ν^m is negligible. Accordingly, only E_1^f and V_F affects the laminate behaviour in terms of first buckling load.

Conversely, since the multilayer plate of benchmark BK2 is characterised by an angle-ply orthotropic symmetric stacking sequence, the first buckling load is influenced by the following properties: E_1^f, E_2^f, E^m and V_F. The sensitivity of the laminate buckling strength to the other elastic properties remains negligible also for this configuration of the plate.

According to the aforementioned remarks, the number of parameters (characterising the material and geometrical properties uncertainty) to be identified varies with the con-

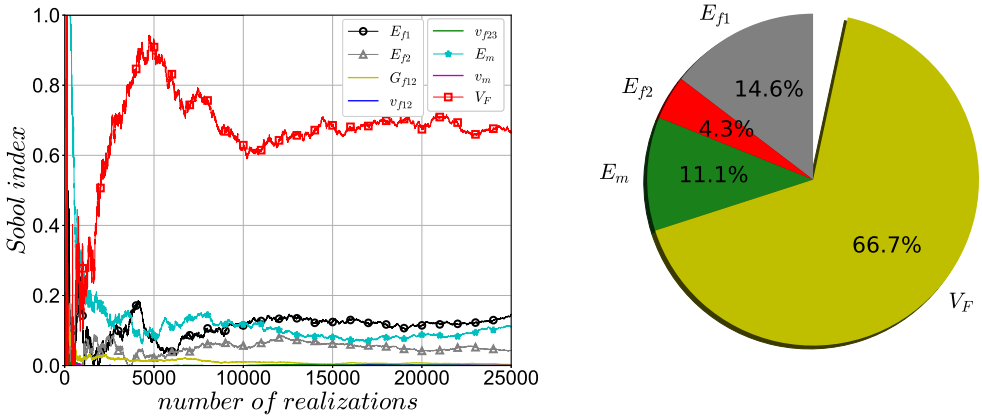

(a) (b)

Figure 7: (a) Convergence of the Sobol index and (b) sensitivity analysis results, for the second benchmark (BK2).

sidered benchmark. These aspects are discussed in detail in the following Section.

6. Mathematical formulation of the inverse problem

6.1. Optimisation variables, objective function and constraints

The multi-scale identification problem is stated as a classical constrained inverse problem: the identification of the elastic properties variability of the composite constitutive phases can be achieved by minimising the Euclidean distance between the reference distribution of the buckling load at macroscopic scale and that resulting from the numerical simulation.

As discussed in Section 5, the sensitivity of the buckling load distribution to the material and geometrical parameters of the microscopic constituents is strongly affected by the stacking sequence of the laminate. Therefore, the number of optimisation variables (i.e. the parameters of the distribution law, for each property at the microscopic scale, to be identified) depends upon the considered benchmark. As a result of the GSA discussed in Section 5, the parameters tuning the distribution of the most relevant elastic and geometrical properties of the constitutive phases can be arranged in the vector of design variables $\boldsymbol{\xi}^{\alpha}$, $(\alpha = \mathrm{BK1}, \mathrm{BK2})$ as follows:

$$\boldsymbol{\xi}^{\mathrm{BK1}} = \left\{ \mu\left(E_1^f\right), \sigma\left(E_1^f\right), \mu\left(V_F\right), \sigma\left(V_F\right) \right\}, \tag{16}$$

$$\boldsymbol{\xi}^{\mathrm{BK2}} = \left\{ \mu\left(E_1^f\right), \sigma\left(E_1^f\right), \mu\left(E_2^f\right), \sigma\left(E_2^f\right), \mu\left(E^m\right), \sigma\left(E^m\right), \mu\left(V_F\right), \sigma\left(V_F\right) \right\}. \tag{17}$$

Accordingly, benchmark BK1 is characterised by four design variables, whilst benchmark BK2 has eight design variables. In both cases, the elastic properties excluded from the vector of design variables (due to the negligible sensitivity of the first buckling load to these quantities) have been set to the reference mean values listed in Table 1.

Each design variable can vary into a suitable definition domain which depends upon the considered benchmark. Lower and upper bounds of design variables for benchmarks BK1 and BK2 are given in Tables 2 and 3, respectively.

Microscopic parameters	Lower bounds	Upper bounds
$\mu\left(E_1^f\right)$ [GPa]	220.8	331.2
$\sigma\left(E_1^f\right)$ [GPa]	22.08	33.12
$\mu\left(V_F\right)$	0.444	0.666
$\sigma\left(V_F\right)$	0.0444	0.0666

Table 2: Benchmark BK1: bounds of the design variables.

Microscopic parameters	Lower bounds	Upper bounds
$\mu\left(E_1^f\right)$ [GPa]	220.8	331.2
$\sigma\left(E_1^f\right)$ [GPa]	22.08	33.12
$\mu\left(E_2^f\right)$ [GPa]	13.84	20.76
$\sigma\left(E_2^f\right)$ [GPa]	1.384	2.076
$\mu\left(E^m\right)$ [GPa]	3.312	4.968
$\sigma\left(E^m\right)$ [GPa]	0.3312	0.4968
$\mu\left(V_F\right)$	0.444	0.666
$\sigma\left(V_F\right)$	0.0444	0.0666

Table 3: Benchmark BK2: bounds of the design variables.

Moreover, in order to ensure the positive definiteness of the stiffness tensors of both the lamina (mesoscopic scale) and the constitutive phases (microscopic scale) [36], every combination of elastic properties generated through the Monte-Carlo technique, must satisfy a set of non-linear constraints $\mathbf{g}\left(\xi^\alpha\right)$ ensuring the positive definiteness of the stiffness tensors [36]. Of course these constraints must be imposed at the lamina-level and at the constitutive phases-level. For the elementary lamina, these constraints read:

$$\begin{aligned}
g_1(\boldsymbol{\xi}^\alpha) &= |\nu_{12}(\boldsymbol{\xi}^\alpha)| - \sqrt{\frac{E_1(\boldsymbol{\xi}^\alpha)}{E_2(\boldsymbol{\xi}^\alpha)}} < 0, \\
g_2(\boldsymbol{\xi}^\alpha) &= |\nu_{23}(\boldsymbol{\xi}^\alpha)| - \sqrt{\frac{E_2(\boldsymbol{\xi}^\alpha)}{E_3(\boldsymbol{\xi}^\alpha)}} < 0, \\
g_3(\boldsymbol{\xi}^\alpha) &= 2\nu_{12}(\boldsymbol{\xi}^\alpha)\nu_{13}(\boldsymbol{\xi}^\alpha)\nu_{23}(\boldsymbol{\xi}^\alpha)\frac{E_3(\boldsymbol{\xi}^\alpha)}{E_1(\boldsymbol{\xi}^\alpha)} + ... \\
&+\nu_{12}(\boldsymbol{\xi}^\alpha)^2\frac{E_2(\boldsymbol{\xi}^\alpha)}{E_1(\boldsymbol{\xi}^\alpha)} + \nu_{23}(\boldsymbol{\xi}^\alpha)^2\frac{E_3(\boldsymbol{\xi}^\alpha)}{E_2(\boldsymbol{\xi}^\alpha)} + \nu_{13}(\boldsymbol{\xi}^\alpha)^2\frac{E_3(\boldsymbol{\xi}^\alpha)}{E_1(\boldsymbol{\xi}^\alpha)} - 1 < 0,
\end{aligned} \tag{18}$$

whilst for the constitutive phases they can be written as

$$\begin{aligned}
g_4(\boldsymbol{\xi}^\alpha) &= |\nu_{12}^f| - \sqrt{\frac{E_1^f(\boldsymbol{\xi}^\alpha)}{E_2^f(\boldsymbol{\xi}^\alpha)^f}} < 0, \\
g_5(\boldsymbol{\xi}^\alpha) &= |\nu_{23}^f| - 1 < 0, \\
g_6(\boldsymbol{\xi}^\alpha) &= \frac{E_1^f(\boldsymbol{\xi}^\alpha)}{E_2^f(\boldsymbol{\xi}^\alpha)}\left[2\nu_{23}^f\left(\nu_{12}^f\right)^2 + 2\left(\nu_{12}^f\right)^2\right] - 1 < 0.
\end{aligned} \tag{19}$$

The objective function $\Phi(\boldsymbol{\xi}^{\alpha})$ is defined as the Euclidean distance between the *reference* and the numerical mechanical response, in terms of the probabilistic parameters $\mu_{buckling}$ and $\sigma_{buckling}$ of the first buckling load. In particular, this objective function is a least-square error estimator defined as:

$$\Phi(\boldsymbol{\xi}^{\alpha}) = \left(\frac{\mu_{buckling}\left(\boldsymbol{\xi}^{\alpha}\right) - \mu_{buckling}^{\mathrm{ref}}}{\mu_{buckling}^{\mathrm{ref}}} \right)^{2} + \left(\frac{\sigma_{buckling}\left(\boldsymbol{\xi}^{\alpha}\right) - \sigma_{buckling}^{\mathrm{ref}}}{\sigma_{buckling}^{\mathrm{ref}}} \right)^{2}. \tag{20}$$

Finally, the multi-scale inverse problem is stated as a classical CNLPP as:

$$\begin{aligned} &\min_{\boldsymbol{\xi}^{\alpha}} \Phi\left(\boldsymbol{\xi}^{\alpha}\right), \\ &\text{subject to:} \\ &g_j\left(\boldsymbol{\xi}^{\alpha}\right) \leq 0, \quad j = 1, ..., 6. \end{aligned} \tag{21}$$

6.2. The numerical strategy

Problem (21) is a non-convex CNLPP, in terms of constraints and objective function. The number of parameters, describing the variability of material and geometrical properties of the constitutive phases, depends on the considered benchmark: the first benchmark (BK1) allows to characterise four parameters, while the second benchmark (BK2) allows to characterise up to eight parameters. Of course, the non-convexity of problem (21) implies the lack of uniqueness of its solution [36].

Taking into account all these aspects, the CNLPP of Eq. (21) is solved by means of a hybrid optimisation tool based on the GA ERASMUS (EvolutionaRy Algorithm for optimiSation of ModUlar Systems), which is interfaced with the MATLAB® *fmincon* algorithm [39], as shown in Figure 8. The GA ERASMUS has already been used successfully to solve different classes of real-world engineering problems [58–66].

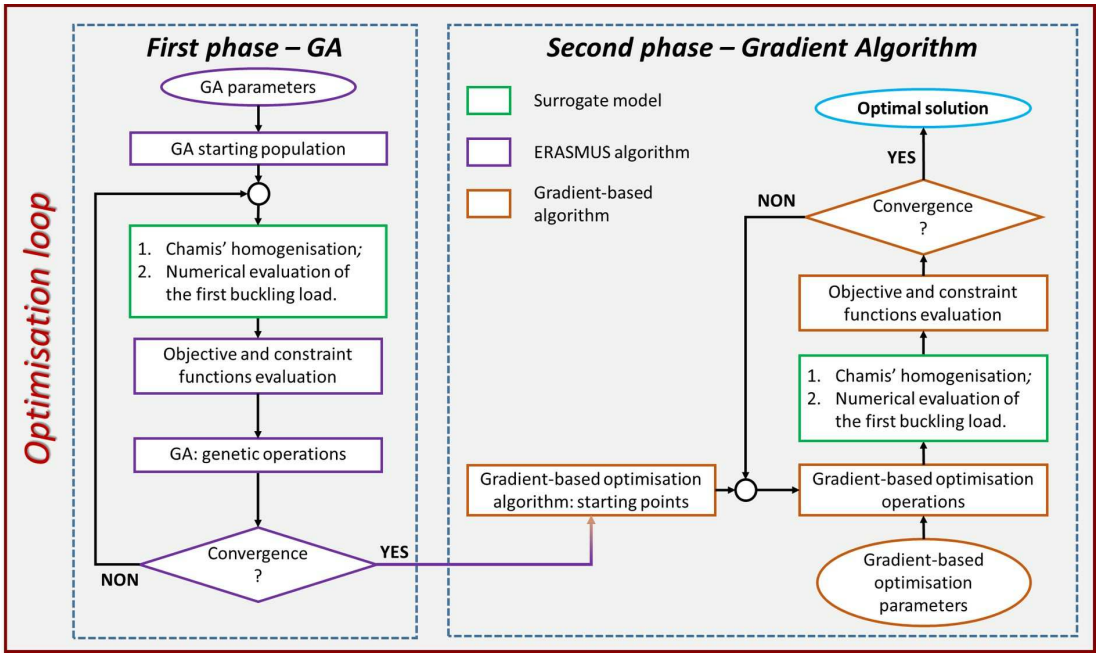

Figure 8: Optimisation strategy for the resolution of problem (21).

The procedure illustrated in Figure 8 is articulated in two phases. The first one represents the global solution search and it is carried out through the GA ERASMUS: the goal is to find potential suboptimal solution which will constitute the starting point for the gradient-based optimisation algorithm. The genotype of the individual is characterised by one chromosome and four genes for the first benchmark (BK1) and eight genes for the second benchmark (BK2).

The second step is the local optimisation phase and it is performed by by means of the MATLAB® *fmincon* tool. The selected optimisation solver is the *active-set* algorithm, i.e. a Quasi-Newton method, in which an approximation of the Hessian matrix is used to compute the descent direction [39].

Each optimisation algorithm has been interfaced to the ANN, presented in Section 4, which emulate both the homogenisation phase and the eigenvalue buckling analysis. The ANN has been employed in order to reduce significantly the computational effort.

In particular, the output of the ANN is the current value of both the objective and the constraint functions which are passed to the optimisation tool in order to execute the optimisation operations: the new microscopic variability parameters and these operations are repeated until the user-defined convergence criteria are met.

7. Numerical results

7.1. Buckling response for the reference configuration

The multi-scale inverse problem defined in Eq. (21) requires the computation of the objective function $\Phi(\boldsymbol{\xi}^{\alpha})$ of Eq. (20): this function depends upon the buckling *reference* response, thus this quantity must be evaluated before starting the optimisation process. Due to the difficulty to get experimental data in terms of variability of the microscopic material properties and the related buckling probability distribution at the macroscopic scale, a numerical test is performed in order to obtain the *reference* data.

To deal with this task the *reference* variability parameters of the material and geometrical properties of the microscopic constituent, listed in Table 1 are considered for each benchmark.

Firstly, a Monte-Carlo simulation is performed to generate randomly a statistically representative number of samples. Secondly, for each sample, the homogenisation step is performed by using the Chamis' model, described in Section 3, to get the lamina elastic properties that are used into the macroscopic FE model, to compute the first buckling load of the plate. After carrying out these operations for the whole set of samples, it is possible to determine the mean value and the relative COV of the first buckling load, according to Eqs. (2) and (3), respectively. The variability parameters of the *reference* first buckling load distribution are then summarised in Table 4: these quantities have been obtained by performing 1000 realisations.

Benchmark	$\mu\left(\sigma^{I}_{buckling}\right)\,[MPa]$	**COV** $\left(\sigma^{I}_{buckling}\right)$
BK1	83.41	0.12
BK2	59.3	0.098

Table 4: Variability parameters of the *reference* first buckling load.

Furthermore, a small sub-set of 20 realisations have been used to train the ANN, for each benchmark. In order to check the accuracy of the ANN, 50 samples generated with the Monte-Carlo technique have been selected as a *validation set* and a comparison

between them and the results provided by the ANN is carried out, as shown in Figure 9 (only the results related to the first benchmark have been reported for the sake of brevity). As a matter of fact, the results provided by the ANN are in very good agreement with the samples constituting the validation set.

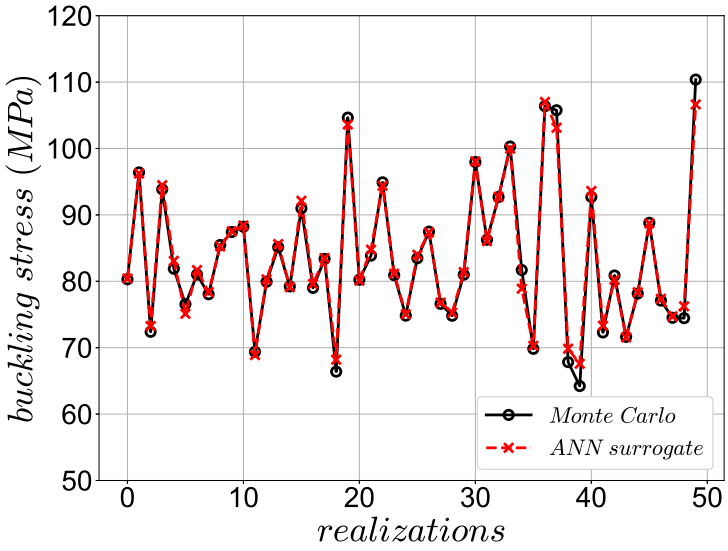

Figure 9: Comparison between the validation set of samples and the results provided by the ANN.

7.2. Numerical results of the MSIS for benchmarks BK1 and BK2

As discussed in Section 2, two benchmarks are investigated in order to show the effectiveness of the proposed MSIS, by varying the stacking sequence of the multilayer plate.

The parameters tuning the GA and the deterministic algorithms are summarised in Tables 5 and 6, respectively, according to the main guidelines described in [67].

Parameters	**BK1**	**BK2**
N. of individuals	40	80
N. of populations	2	2
N. of iterations	100	100
Crossover probability.	0.85	0.85
Mutation probability.	0.025	0.0125
Isolation time	20	20

Table 5: Optimisation parameters for the genetic algorithm, for benchmarks BK1 and BK2.

Parameters	**BK1**	**BK2**
Solver	active-set	active-set
Max n. of function evaluation	10000	10000
Tol. on the objective function	10^{-15}	10^{-15}
Tol. on the gradient norm	10^{-15}	10^{-15}

Table 6: Optimisation parameters for the gradient-based algorithm, for benchmarks BK1 and BK2.

The GA calculation is performed with two populations, in which, the number of individuals, evolving along the selected maximum number of generations, depends on the considered benchmark. Indeed, the best practice is to set the number of individuals greater than or equal to ten times the number of optimisation variables. Accordingly, benchmarks BK1 and BK2 are characterised by two populations composed of 40 and 80 individuals, respectively. The two populations exchange the best individual every ten iterations, by using a ring-type operator, whose probability is automatically computed by the considered GA. Moreover, as far as the constraint-handling technique is concerned, the Automatic Dynamic Penalisation (ADP) method is used [68].

It is noteworthy that, the choice of multiple populations, with a small number of individuals, allows finding the global minimum without increasing too much the computational effort. In this way, the GA has the possibility to explore the design domain in the most effective way, by exchanging information between the best individuals belonging to each population: the reader is addressed to [37] for more details about these aspects.

Since, the proposed strategy makes use of a metaheuristic algorithm, the GA is run three times for each benchmark. The best individual obtained at the end of the genetic calculation is used as a starting guess for the gradient-based algorithm, in order to execute the subsequent local optimisation.

In terms of computational effort, the training phase of the ANN needs several seconds to be performed. Then, the hybrid optimisation strategy needs 37.8 and 68.2 hours for the benchmarks BK1 and BK2, respectively, on an Intel® Xeon® 2.70 GHz CPU with two processors and with a RAM of 128 GB.

The results provided by the ERASMUS GA for benchmarks BK1 and BK2 are summarised in Tables 7and 9, respectively, whilst those provided by the gradient-based algorithm are reported in Tables 8 and 10, respectively. In order to compare the obtained results with the *reference* ones, the average of the gradient-based algorithm solutions is performed for each identified parameter, as it can be seen in Tables 8 and 10, for each benchmark.

As it can be easily inferred from the analysis of these results, the mean value and the standard deviation of the microscopic material properties are in good agreement with the *reference* data: the absolute percentage error ranges from 2.8% to 13.4% for the first benchmark and from 0.2% to 3.2% for the second benchmark.
The discrepancy between the values of $\mu\left(E_1^f\right)$ and $\mu\left(V_F\right)$ provided by the MSIS and the reference ones, for benchmark BK1, is related to the nature of the laminate stack. Indeed, for this benchmark, the considered sequence has an isotropic membrane stiffness matrix but a completely anisotropic bending stiffness matrix. This aspect has a strong influence on the solution search for the multi-scale inverse problem because the first buckling load is dominated by the bending stiffness of the laminate. In particular, if the bending stiffness matrix is not orthotropic, problem (21) becomes strongly non-convex and several equivalent optimal solutions exist. Therefore, finding the global minimum is anything but trivial in such a case.
These results prove that a particular care should be put in the choice of the stacking sequence, which strongly affect both the number of parameters that is possible to identify and the quality of the final result.

8. Conclusions

In this work the multi-scale identification strategy (MSIS), initially presented in [36], has been extended to the characterisation of the uncertainty of the geometrical and elastic

Analysis name	$\mu\left(E_1^f\right)[GPa]$	$\sigma\left(E_1^f\right)[GPa]$	$\mu(V_F)$	$\sigma(V_F)$
REF	276	27.6	0.555	0.0555
GE1A	238	27.1	0.628	0.0562
GE1B	237	27.1	0.630	0.0562
GE1C	237	27.1	0.630	0.0564
GE2A	257	25.5	0.589	0.0595
GE2B	257	25.5	0.589	0.0595
GE2C	257	25.4	0.589	0.0597
GE3A	221	25.3	0.665	0.0597
GE3B	223	25.5	0.662	0.0593
GE3C	223	25.5	0.661	0.0593

Table 7: Optimum solution of the multi-scale inverse problem provided by the GA, for benchmark BK1.

Analysis name	$\mu\left(E_1^f\right)[GPa]$	$\sigma\left(E_1^f\right)[GPa]$	$\mu(V_F)$	$\sigma(V_F)$	$\Phi(\mathbf{x})$
REF	276	27.6	0.555	0.0555	0
GR1A	238	27.1	0.625	0.0564	3.01E-05
GR1B	244	27.6	0.616	0.0567	5.58E-07
GR1C	235	27.1	0.632	0.0526	1.62E-05
GR2A	257	25.6	0.588	0.0594	7.33E-06
GR2B	257	25.5	0.589	0.0596	3.00E-07
GR2C	255	25.2	0.594	0.0586	2.88E-07
GR3A	221	25.3	0.665	0.0597	2.48E-07
GR3B	223	27.1	0.663	0.0512	2.11E-06
GR3C	223	25.5	0.661	0.0593	7.37E-08
AVERAGE	239 (-13.4)	26.2 (-5)	0.626 (12.8)	0.0571 (2.8)	

Table 8: Optimum solution of the multi-scale inverse problem provided by the gradient-based algorithm, for benchmark BK1; the percentage difference between the solution and the microscopic *reference* data are given in parentheses.

Analysis name	$\mu\left(E_1^f\right)[GPa]$	$\sigma\left(E_1^f\right)[GPa]$	$\mu\left(E_2^f\right)[GPa]$	$\sigma\left(E_2^f\right)[GPa]$	$\mu\left(E^m\right)[GPa]$	$\sigma\left(E^m\right)[GPa]$	$\mu\left(V_F\right)$	$\sigma\left(V_F\right)$
REF	276	27.6	17.3	1.73	4.14	0.414	0.555	0.0555
GE1A	255	31.2	15.7	1.50	3.64	0.412	0.620	0.0540
GE1B	311	30.3	20.1	2.02	4.49	0.366	0.482	0.0547
GE1C	313	30.2	20.0	1.59	4.47	0.363	0.482	0.0554
GE2A	304	22.4	18.3	1.51	3.43	0.484	0.568	0.0523
GE2B	304	22.4	18.3	1.51	3.43	0.484	0.568	0.0523
GE2C	258	24.5	16.0	1.93	4.23	0.467	0.581	0.0593
GE3A	233	24.8	16.0	1.59	4.16	0.404	0.615	0.0633
GE3B	233	24.8	16.0	1.59	4.16	0.409	0.615	0.0632
GE3C	233	24.8	16.0	1.60	4.16	0.404	0.615	0.0633

Table 9: Optimum solution of the multi-scale inverse problem provided by the GA, for benchmark BK2.

Analysis name	$\mu\left(E_1^f\right)[GPa]$	$\sigma\left(E_1^f\right)[GPa]$	$\mu\left(E_2^f\right)[GPa]$	$\sigma\left(E_2^f\right)[GPa]$	$\mu\left(E^m\right)[GPa]$	$\sigma\left(E^m\right)[GPa]$	$\mu\left(V_F\right)$	$\sigma\left(V_F\right)$	$\Phi(\mathbf{x})$
REF	276	27.6	17.3	1.73	4.14	0.414	0.555	0.0555	0
GR1A	288	31.3	17.7	1.74	4.24	0.433	0.520	0.0514	4.50E-04
GR1B	280	28.8	18.8	1.75	4.33	0.401	0.529	0.0539	1.77E-06
GR1C	306	29.4	19.5	1.58	4.38	0.377	0.497	0.0548	4.27E-07
GR2A	288	31.3	17.7	1.74	4.24	0.433	0.520	0.0514	1.71E-09
GR2B	304	22.4	18.3	1.51	3.43	0.484	0.568	0.0523	3.59E-08
GR2C	258	26.1	16.4	1.96	4.14	0.450	0.569	0.0579	2.76E-04
GR3A	236	24.7	16.0	1.61	4.14	0.402	0.610	0.0634	2.05E-05
GR3B	233	24.8	16.0	1.59	4.16	0.409	0.615	0.0632	1.45E-07
GR3C	233	24.7	16.2	1.59	4.14	0.407	0.617	0.0634	1.98E-07
AVERAGE	270 (-2.3)	27 (-2)	17.4 (0.5)	1.67 (-3.2)	4.13 (-0.2)	0.422 (1.9)	0.561 (1)	0.0569 (2.5)	

Table 10: Optimum solution of the multi-scale inverse problem provided by the gradient-based algorithm, for benchmark BK2; the percentage difference between the solution and the microscopic *reference* data are given in parentheses.

properties of the fibre and the matrix at the microscopic scale, by using information restrained in the macroscopic response of the laminate, i.e. the first buckling load of the multilayer plate.

In this context, the multi-scale characterisation problem, is stated as a constrained inverse problem. The goal is the minimisation of the distance between the numerical and the reference variability parameters that describe the probability distribution of the first buckling load. In this case, the solution search is performed by a hybrid optimisation tool, in which, a metaheuristic algorithm and a gradient-based one have been interfaced to solve the related non-convex CNLPP.

The MSIS makes use of an analytical homogenisation scheme, i.e. the Chamis' model, to perform the microscopic / mesoscopic scale transition. The elastic properties of the elementary lamina evaluated by means of the Chamis' model are then used into the FE model of multilayer plate to evaluate its first buckling load.

Moreover, a Monte-Carlo simulation campaign has been performed to compute the probability distribution of the first buckling load, starting from a Gaussian probability distribution of the material properties of the constituent phases. The obtained samples have been used to train an ANN which emulates the multi-scale mechanical response of the plate: the inputs are the geometrical and elastic properties of the microscopic constituents of the composite and the output is the first-buckling load of the laminate. Then, the obtained surrogate model has been used into the optimisation process to reduce the computational effort.

Before executing the hybrid optimisation process, a sensitivity study has been performed to determine the most relevant microscopic parameters influencing the first buckling load at the macroscopic scale. In particular, numerical results show that this sensitivity is strongly affected by the nature of the stacking sequence. Therefore to prove the effectiveness of the proposed MSIS two different stacking sequences have been considered: the first benchmark is characterised by a symmetric quasi-isotropic stack, while the second one is characterised by a symmetric orthotropic one.

As a consequence, also the obtained results, in terms of the identifiction of the parameters tuning the variability of the elastic and geometrical properties of the constitutive phases of the composite, are strongly influenced by the nature of the laminate lay-up. In particular, for the first benchmark the absolute percentage error ranges from 2.8% to 13.4% for the standard deviation of the fibre volume fraction $\sigma\left(V_F\right)$ and the mean value of the fibre longitudinal elastic modulus $\mu\left(E_1^f\right)$, respectively. Conversely, for the second benchmark the absolute percentage error ranges from 0.2% to 3.2% for the mean value of the matrix elastic modulus $\mu\left(E^m\right)$ and the standard deviation of the fibre transverse elastic modulus $\sigma\left(E_2^f\right)$.

Nevertheless, thanks to the proposed MSIS, it is possible to retrieve the variability of both longitudinal and transversal effective properties of the constitutive phases and this task cannot be easily performed by means of standard ASTM tests.

As far as perspectives of this work are concerned, research is ongoing, in order to include into the MSIS the following aspects:

- the validation of the MSIS by means of experimental data. In this case, the influence of noise on the results provided by the MSIS should be properly taken into account. To this purpose, suitable regularisation techniques, as the Tikhonov-Morozov one, which is widely used in different engineering fields [69, 70], must be efficiently integrated into the multi-scale identification process to handle noise;

- the formulation of a suitable optimisation problem to find a suitable stack which maximise the sensitivity of the first buckling load to each parameter defined at the microscopic scale of the composite;
- the extension of the MSIS to the characterisation of the variability of the viscoelastic properties of the microscopic constituent and the evaluation of the variability effects related to further geometrical parameters, e.g. fibre misalignment, macroscopic geometrical defects, etc.

Finally, thanks to the versatility of the proposed MSIS, it is possible to increase the accuracy in terms of variability parameters by introducing more general probability density functions for both the buckling load and the microscopic parameters. In this way, it will be possible to go beyond the limit of the Gaussian model, in which the shape of the distribution is imposed a priori.

Acknowledgements

This research work has been carried out within the project FULLCOMP (FULLy analysis, design, manufacturing, and health monitoring of COMPosite structures), funded by the European Union Horizon 2020 Research and Innovation program under the Marie Skodowska-Curie grant agreement No. 642121.

References

[1] R. M. Jones, Mechanics of composite materials, McGraw-Hill, 1975.

[2] M. F. Funari, F. Greco, P. Lonetti, R. Luciano, R. Penna, An interface approach based on moving mesh and cohesive modeling in z-pinned composite laminates, Composites Part B: Engineering 135 (2018) 207 – 217. doi:https://doi.org/10.1016/j.compositesb.2017.10.018.

[3] M. F. Funari, F. Greco, P. Lonetti, A moving interface finite element formulation for layered structures, Composites Part B: Engineering 96 (2016) 325 – 337. doi:https://doi.org/10.1016/j.compositesb.2016.04.047.

[4] M. F. Funari, F. Greco, P. Lonetti, A numerical model based on ALE formulation to predict crack propagation in sandwich structures, Fracture and Structural Integrity: ten years of Frattura ed Integrit Strutturale 47 (2019) 277–293. doi:https://doi.org/10.3221/IGF-ESIS.47.21.

[5] S. Naskar, T. Mukhopadhyay, S. Sriramula, Probabilistic micromechanical spatial variability quantification in laminated composites, Composites Part B: Engineering 151 (2018) 291 – 325. doi:https://doi.org/10.1016/j.compositesb.2018.06.002.

[6] K. Sepahvand, S. Marburg, Identification of composite uncertain material parameters from experimental modal data, Probabilistic Engineering Mechanics 37 (2014) 148 – 153. doi:https://doi.org/10.1016/j.probengmech.2014.06.008.

[7] ASTM International, West Conshohocken, PA, ASTM D3039 / D3039M-17, Standard Test Method for Tensile Properties of Polymer Matrix Composite Materials (2017).

[8] ASTM International, West Conshohocken, PA, ASTM D790-17, Standard Test Methods for Flexural Properties of Unreinforced and Reinforced Plastics and Electrical Insulating Materials (2017).

[9] ASTM International, West Conshohocken, PA, ASTM D3410 / D3410M-16, Standard Test Method for Compressive Properties of Polymer Matrix Composite Materials with Unsupported Gage Section by Shear Loading (2016).

[10] ASTM International, West Conshohocken, PA, ASTM D5379 / D5379M-12, Standard Test Method for Shear Properties of Composite Materials by the V-Notched Beam Method (2012).

[11] ASTM International, West Conshohocken, PA, ASTM D7078 / D7078M-12, Standard Test Method for Shear Properties of Composite Materials by V-Notched Rail Shear Method (2012).

[12] ASTM International, West Conshohocken, PA, ASTM D3518 / D3518M-13, Standard Test Method for In-Plane Shear Response of Polymer Matrix Composite Materials by Tensile Test of a 45 Laminate (2013).

[13] ASTM International, West Conshohocken, PA, ASTM D2344 / D2344M-16, Standard Test Method for Short-Beam Strength of Polymer Matrix Composite Materials and Their Laminates (2016).

[14] ASTM International, West Conshohocken, PA, ASTM D3379-75(1989)e1, Standard Test Method for Tensile Strength and Young's Modulus for High-Modulus Single-Filament Materials (Withdrawn 1998) (1975).

[15] ASTM International, West Conshohocken, PA, ASTM D638-14, Standard Test Method for Tensile Properties of Plastics (2014).

[16] J. A. Nairn, Analytical fracture mechanics analysis of the pull-out test including the effects of friction and thermal stresses, Advanced Composite Letters 9 (6) (2000) 373–383.

[17] R. Maurin, P. Davies, N. Baral, C. Baley, Transverse Properties of Carbon Fibres by Nano-Indentation and Micro-mechanics, Applied Composite Materials 15 (2018) 61–73.

[18] S. Feih, K. Wonsyld, D. Minzari, P. Westermann, H. Lilholt, Testing Procedure for the Single Fiber Fragmentation Test, Vol. No. 1483(EN), Denmark. Forskningscenter Risoe. Risoe-R, 2004.

[19] K. Sepahvand, S. Marburg, On construction of uncertain material parameter using generalized polynomial chaos expansion from experimental data, Procedia IUTAM 6 (2013) 4 – 17, iUTAM Symposium on Multiscale Problems in Stochastic Mechanics. doi:https://doi.org/10.1016/j.piutam.2013.01.001.

[20] O. Pajonk, B. V. Rosi, A. Litvinenko, H. G. Matthies, A deterministic filter for non-gaussian bayesian estimation applications to dynamical system estimation with noisy measurements, Physica D: Nonlinear Phenomena 241 (7) (2012) 775 – 788. doi:https://doi.org/10.1016/j.physd.2012.01.001.

[21] C. Desceliers, R. Ghanem, C. Soize, Maximum likelihood estimation of stochastic chaos representations from experimental data, International Journal for Numerical Methods in Engineering 66 (6) (2006) 978–1001. doi:10.1002/nme.1576.

[22] Y. M. Marzouk, H. N. Najm, L. A. Rahn, Stochastic spectral methods for efficient bayesian solution of inverse problems, Journal of Computational Physics 224 (2) (2007) 560 – 586. doi:https://doi.org/10.1016/j.jcp.2006.10.010.

[23] C. Soize, A computational inverse method for identification of non-gaussian random fields using the bayesian approach in very high dimension, Computer Methods in Applied Mechanics and Engineering 200 (45) (2011) 3083 – 3099. doi:https://doi.org/10.1016/j.cma.2011.07.005.

[24] V. A. B. Narayanan, N. Zabaras, Stochastic inverse heat conduction using a spectral approach, International Journal for Numerical Methods in Engineering 60 (9) (2004) 1569–1593. doi:10.1002/nme.1015.

[25] C. Proppe, Reliability computation with local polynomial chaos approximations, ZAMM - Journal of Applied Mathematics and Mechanics / Zeitschrift fr Angewandte Mathematik und Mechanik 89 (1) (2009) 28–37. doi:10.1002/zamm.200800072.

[26] A. Batou, C. Soize, Stochastic modeling and identification of an uncertain computational dynamical model with random fields properties and model uncertainties, Arch Appl Mech (2012) 1–18.

[27] J. Wang, N. Zabaras, Hierarchical bayesian models for inverse problems in heat conduction, Inverse Problems 21 (1) (2004) 183–206. doi:10.1088/0266-5611/21/1/012.

[28] R. G. Ghanem, A. Doostan, On the construction and analysis of stochastic models: Characterization and propagation of the errors associated with limited data, Journal of Computational Physics 217 (1) (2006) 63 – 81, uncertainty Quantification in Simulation Science. doi:https://doi.org/10.1016/j.jcp.2006.01.037.

[29] C. Chen, D. Duhamel, C. Soize, Probabilistic approach for model and data uncertainties and its experimental identification in structural dynamics: Case of composite sandwich panels, Journal of Sound and Vibration 294 (1) (2006) 64 – 81. doi:https://doi.org/10.1016/j.jsv.2005.10.013.

[30] B. V. Rosi, A. Litvinenko, O. Pajonk, H. G. Matthies, Sampling-free linear bayesian update of polynomial chaos representations, Journal of Computational Physics 231 (17) (2012) 5761 – 5787. doi:https://doi.org/10.1016/j.jcp.2012.04.044.

[31] N. Vu-Bac, R. Rafiee, X. Zhuang, T. Lahmer, T. Rabczuk, Uncertainty quantification for multiscale modeling of polymer nanocomposites with correlated parameters, Composites Part B: Engineering 68 (2015) 446 – 464. doi:https://doi.org/10.1016/j.compositesb.2014.09.008.

[32] E. J. Riley, K. L. Koudela, R. M. Narayanan, Characterization of the electromagnetic parameter uncertainty in single-ply unidirectional carbon-fiber-reinforced-polymer laminas, Composites Part B: Engineering 162 (2019) 361 – 368. doi:https://doi.org/10.1016/j.compositesb.2018.10.089.

[33] S. Dey, T. Mukhopadhyay, S. Sahu, G. Li, H. Rabitz, S. Adhikari, Thermal uncertainty quantification in frequency responses of laminated composite plates, Composites Part B: Engineering 80 (2015) 186 – 197. doi:https://doi.org/10.1016/j.compositesb.2015.06.006.

[34] C. Dong, Uncertainties in flexural strength of carbon/glass fibre reinforced hybrid epoxy composites, Composites Part B: Engineering 98 (2016) 176 – 181. doi:https://doi.org/10.1016/j.compositesb.2016.05.035.

[35] M. A. Alazwari, S. S. Rao, Modeling and analysis of composite laminates in the presence of uncertainties, Composites Part B: Engineering 161 (2019) 107 – 120. doi:https://doi.org/10.1016/j.compositesb.2018.10.052.

[36] L. Cappelli, M. Montemurro, F. Dau, L. Guillaumat, Characterisation of composite elastic properties by means of a multi-scale two-level inverse approach, Composite Structures 204 (2018) 767 – 777. doi:https://doi.org/10.1016/j.compstruct.2018.08.007.

[37] M. Montemurro, A contribution to the development of design strategies for the optimisation of lightweight structures, Hdr thesis, Université de Bordeaux (2018).

[38] M. Montemurro, Optimal Design of Advanced Engineering Modular Systems through a New Genetic Approach, Ph.D. thesis, UPMC, Paris VI, France (2012).
URL http://tel.archives-ouvertes.fr/tel-00955533

[39] The MathWorks, Inc., 3 Apple Ill Drive, Natick, MA 01760-2098, Optimization Toolbox User's Guide (2017).

[40] C. C. Chamis, Mechanics of composite materials: Past, present, and future, Journal of Composites Technology and Research 11 (1) (1989) 3–14.

[41] G. Balokas, S. Czichon, R. Rolfes, Neural network assisted multiscale analysis for the elastic properties prediction of 3d braided composites under uncertainty, Composite Structures 183 (2018) 550 – 562. doi:https://doi.org/10.1016/j.compstruct.2017.06.037.

[42] G. Schuller, H. Jensen, Computational methods in optimization considering uncertainties an overview, Computer Methods in Applied Mechanics and Engineering 198 (1) (2008) 2 – 13. doi:https://doi.org/10.1016/j.cma.2008.05.004.

[43] I. Enevoldsen, J. Srensen, Reliability-based optimization in structural engineering, Structural Safety 15 (3) (1994) 169 – 196. doi:https://doi.org/10.1016/0167-4730(94)90039-6.

[44] M. Gasser, G. Schuller, Reliability-based optimization of structural systems, Mathematical Methods of Operations Research 46 (3) (1997) 287 – 307. doi:https://doi.org/doi.org/10.1007/BF01194858.

[45] H. A. Jensen, Design and sensitivity analysis of dynamical systems subjected to stochastic loading, Computers & Structures 83 (14) (2005) 1062 – 1075. doi:https://doi.org/10.1016/j.compstruc.2004.11.016.

[46] M. Papadrakakis, N. Lagaros, V. Plevris, Design optimization of steel structures considering uncertainties, Engineering Structures 27 (9) (2005) 1408 – 1418. doi:https://doi.org/10.1016/j.engstruct.2005.04.002.

[47] I. Doltsinis, Z. Kang, Robust design of structures using optimization methods, Computer Methods in Applied Mechanics and Engineering 193 (23) (2004) 2221 – 2237. doi:https://doi.org/10.1016/j.cma.2003.12.055.

[48] C. Farhat, F. Hemez, Updating finite element dynamic models using an element-by-element sensitivity methodology, American Institute of Aeronautics and Astronautics 31 (9) (1993) 1702–1711. doi:https://doi.org/10.2514/3.11833.

[49] F. M. Hemez, S. W. Doebling, Review and assessment of model updating for non-linear, transient dynamics, Mechanical Systems and Signal Processing 15 (1) (2001) 45 – 74. doi:https://doi.org/10.1006/mssp.2000.1351.

[50] C. Soutis, P. W. R. Beaumont (Eds.), Multi-scale modelling of composite material systems. The art of predictive damage modelling, Woodhead Publishing Series in Composites Science and Engineering, Elsevier, New York, 2005.

[51] Hexcell Corporation, Hexply F584 (2016).

[52] L. Feo, F. Greco, L. Leonetti, R. Luciano, Mixed-mode fracture in lightweight aggregate concrete by using a moving mesh approach within a multiscale framework, Composite Structures 123 (2015) 88 – 97. doi:https://doi.org/10.1016/j.compstruct.2014.12.037.

[53] D. Bruno, F. Greco, R. Luciano, P. N. Blasi, Nonlinear homogenized properties of defected composite materials, Computers & Structures 134 (2014) 102 – 111. doi:https://doi.org/10.1016/j.compstruc.2013.11.018.

[54] E. Barbero, Finite element analysis of composite materials, CRC Press, Taylor and Francis Group, 2007.

[55] D. Systme, Abaqus Analysis User's Guide, Dassault Systmes Simulia Corp., Providence, RI, USA (2013).

[56] I. M. Sobol, Global sensitivity indices for nonlinear mathematical models and their Monte Carlo estimates, Mathematics and Computers in Simulation 55(1-3) (1-3) (2001) 271 – 28. doi:https://doi.org/10.1016/S0378-4754(00)00270-6.

[57] S. Dey, T. Mukhopadhyay, S. Adhikari, Metamodel based high-fidelity stochastic analysis of composite laminates: A concise review with critical comparative assessment, Composite Structures 171 (2017) 227 – 250. doi:https://doi.org/10.1016/j.compstruct.2017.01.061.

[58] M. Montemurro, A. Catapano, D. Doroszewski, A multi-scale approach for the simultaneous shape and material optimisation of sandwich panels with cellular core, Composites Part B: Engineering 91 (2016) 458 – 472. doi:https://doi.org/10.1016/j.compstruct.2014.07.058.

[59] M. Montemurro, A. Catapano, On the effective integration of manufacturability constraints within the multi-scale methodology for designing variable angle-tow laminates, Composite Structures 161 (2017) 145 – 159. doi:https://doi.org/10.1016/j.compstruct.2016.11.018.

[60] M. Montemurro, A. Catapano, A general B-Spline surfaces theoretical framework for optimisation of variable angle-tow laminates, Composite Structures 209 (2019) 561 – 578. doi:https://doi.org/10.1016/j.compstruct.2018.10.094.

[61] G. Costa, M. Montemurro, J. Pailhs, A General Hybrid Optimization Strategy for Curve Fitting in the Non-Uniform Rational Basis Spline Framework, Journal of Optimization Theory and Applications 176 (1) (2018) 225 – 251. doi:https://doi.org/10.1007/s10957-017-1192-2.

[62] M. Montemurro, M. I. Izzi, J. El-Yagoubi, D. Fanteria, Least-weight composite plates with unconventional stacking sequences: Design, analysis and experiments, Journal of Composite Materialsdoi:10.1177/0021998318824783.

[63] E. Panettieri, M. Montemurro, A. Catapano, Blending constraints for composite laminates in polar parameters space, Composites Part B: Engineering 168 (2019) 448 – 457. doi:https://doi.org/10.1016/j.compositesb.2019.03.040.

[64] G. Bertolino, M. Montemurro, G. D. Pasquale, Multi-scale shape optimisation of lattice structures : an evolutionary-based approach, International Journal on Interactive Design and Manufacturingdoi:https://doi.org/10.1007/s12008-019-00580-9.

[65] Y. Audoux, M. Montemurro, J. Pailhes, A surrogate model based on non-uniform rational b-splines hypersurfaces, Procedia CIRP 70 (2018) 463 – 468, 28th CIRP Design Conference 2018, 23-25 May 2018, Nantes, France. doi:https://doi.org/10.1016/j.procir.2018.03.234.

[66] T. Garulli, A. Catapano, M. Montemurro, J. Jumel, D. Fanteria, Quasi-trivial stacking sequences for the design of thick laminates, Composite Structures 200 (2018) 614 – 623. doi:https://doi.org/10.1016/j.compstruct.2018.05.120.

[67] M. Montemurro, H. Nasser, Y. Koutsawa, S. Belouettar, A. Vincenti, P. Vannucci, Identification of electromechanical properties of piezoelectric structures through evolutionary optimisation techniques, International Journal of Solids and Structures 49 (13) (2012) 1884 – 1892.

[68] M. Montemurro, A. Vincenti, P. Vannucci, The automatic dynamic penalisation method (ADP) for handling constraints with genetic algorithms, Computer Methods in Applied Mechanics and Engineering 256 (2013) 70 – 87.

[69] S. A. Faghidian, Inverse determination of the regularized residual stress and eigenstrain fields due to surface peening, The Journal of Strain Analysis for Engineering Design 50 (2) (2015) 84–91. doi:10.1177/0309324714558326.

[70] S. A. Faghidian, A regularized approach to linear regression of fatigue life measurements, International Journal of Structural Integrity 7 (1) (2016) 95–105. doi:10.1108/IJSI-12-2014-0071.